A Fixed-Lag Particle Filter for the Joint Detection/Compensation of Interference Effects in GPS Navigation

Audrey Giremus, Jean-Yves Tourneret, Arnaud Doucet

A Fixed-lag Particle Filter for the Joint Detection/Compensation of Interference Effects in GPS Navigation

Audrey Giremus, Jean-Yves Tourneret, *Senior Member, IEEE* and Arnaud Doucet

***Abstract*—Interferences are among the most penalizing error sources in Global Positioning System (GPS) navigation. So far, many effort has been devoted to developing GPS receivers more robust to the radio-frequency environment. Contrary to previous approaches, this paper does not aim at improving the estimation of the GPS pseudo-distances between the mobile and the GPS satellites in the presence of interferences. As an alternative, we propose to model interference effects as variance jumps affecting the GPS measurements which can be directly detected and compensated at the level of the navigation algorithm. Since the joint detection/estimation of the interference errors and motion parameters is a highly non linear problem, a particle filtering technique is used. An original particle filter is developed to improve the detection performance while ensuring a good accuracy of the positioning solution.**

***Index Terms*—GPS navigation, interferences, particle filtering, smoothing, hypothesis test.**

I. Introduction

First developed in the eighties for military purposes, the global positioning system (GPS) is used nowadays in a variety of applications ranging from the most stringent ones such as civil aviation to mass-market mobile phone positioning services. GPS is a radionavigation system which relies on radio-frequency (RF) signals emitted by a constellation of satellites. As a consequence, it is vulnerable to RF interferences. These interferences can severely impair navigation accuracy and even result in a temporary loss of the GPS service.

More precisely, GPS is based on direct-sequence spread-spectrum coding. By exploiting the correlation properties of the sequences spreading the satellite signals, GPS receivers can acquire and track their propagation delays. Then, four times of transmission allow one to compute the three spatial coordinates of the receiver as well as its clock offset with respect to a reference time. A consequence of interferences is to decrease the signal to noise ratio (SNR) of the GPS signal and thereby to increase the uncertainty on the delay estimates. If the SNR is reduced below the receiver tracking threshold, the receiver loses its ability to obtain measurements from the satellites. As these interferences are moreover unpredictable, they are one of the most penalizing sources of error, along with multipaths, in GPS navigation.

Interference mitigation has been an active research topic for many years. RF interferences originate from different sources and can take different forms such as wideband noise, continuous waves, pulsed noise or frequency hopping. Special attention has been paid to designing receiver enhancements to discriminate the GPS signal from parasite signals. Conventional approaches include filtering in the three domains, i.e. spatial, temporal and frequential [32]. Filtering can be applied at different stages of the receiver. Pre-filtering of the GPS signals has proved efficient against out-of-band interferences. However, filters with a sharp cutoff are difficult to design at high frequencies [31]. Another solution consists of narrowing the bandwidth of the tracking loop filters. Thus, the robustness to interferences is improved but the tolerance of the receiver to high dynamics is decreased. To obviate this limitation, external aiding to the receiver can be used. It can be provided for instance by inertial navigation systems (INS) which are immune to the navigation RF environment. More precisely, by providing prior estimates of the line-of-sight distances between the receiver and the satellites, INS allow one to remove dynamic stress from the tracking loop [2]. As a complement to these approaches, multiple antenna arrays have been paid lately a lot of attention. The principle is to modify the antenna pattern by setting to zero the assumed directions of interference sources. For that purpose, adaptive beamforming and high resolution finding methods are used [26]. A comprehensive review of existing design solutions can be found in [17].

Unlike the above-mentioned methods, our purpose is not to enhance the GPS signal SNR but to compensate directly for interference effects at the level of the navigation algorithm. In this way, the structure of GPS receiver can be left unchanged. Thus, our study considers low power interferences which do not result in a receiver loss of lock but still degrade the navigation solution. To our knowledge, it is the first time such an approach is applied to mitigate RF perturbations. Similar techniques have been developed in the civil aviation community to monitor the integrity of the GPS measurements. However, the so-called fault detection and exclusion (FDE) algorithms [7] [18] [29] are intended to cope with bias or ramp errors whereas interferences more likely result in variance jumps [5]. In addition, they generally make the assumption of a single faulty measurement at a time to perform exclusion. Our contribution is threefold. First, our algorithm is

A. Giremus is with the University of Bordeaux, IMS-LAPS-UMR 5218, Talence, France, e-mail: audrey.giremus@laps.ims-bordeaux.fr.

J.-Y. Tourneret is with the University of Toulouse, IRIT-ENSEEIHT-TéSA, France, e-mail: jean-yves.tourneret@enseeiht.fr.

A. Doucet is with the Institute of Statistical Mathematics, Tokyo, Japan, e-mail: arnaud@ism.ac.jp.

dedicated to variance jump detection. Second, it can handle several corrupted measurements at a time. Finally, instead of excluding the faulty measurements, we estimate the value of the observation noise variance in the presence of interferences so as not to discard useful information to solve the positioning problem. Jointly detecting the variance jumps and estimating their values together with the dynamics of the mobile is a highly non linear problem. Therefore, we consider in this paper a fully Bayesian approach based on particle filtering (PF). By noting that several consecutive GPS measurements are usually affected by a given source of interferences, we consider a fixed-lag PF (FLPF) smoother to ease interference detection. Indeed, FLPF have the advantage of delaying the estimation to make use of information from near future observations as outlined in [30]. It should be noted that such a strategy has already proved useful to address the problem of multipath in GPS navigation [15]. With the same concern for performance, we propose several modifications to a standard PF algorithm. Basically, PF consist of propagating a set of possible solutions to the estimation problem, called particles. Each of them is assigned a weight approximately proportional to its posterior probability. In this paper, a suboptimal but analytically tractable distribution is proposed to sample particles conditional on near future observations. In addition, the prior probability for a variance jump is adjusted so as to favor a minimal delay between two consecutive detections and thus prevent false alarms. Finally, removal of non relevant particles is sped up by penalizing them on the basis of an hypothesis test.

The remainder of the paper is organized as follows. Section II presents the GPS navigation model in the presence of interferences. Section III is dedicated to the Bayesian modeling of the problem. Section IV details the proposed PF for navigation in the presence of interferences. We emphasize the different improvements introduced with regards to a classical PF. Finally, simulation results illustrate the performance of the approach in section V. Conclusions are reported in section VI.

II. GPS MEASUREMENT MODEL

GPS receivers compute the position of a mobile by triangulation from distance measurements to satellites of known locations. These satellite to receiver ranging are computed by multiplying the estimated propagation delays of satellite signals by the speed of light $c = 3 \times 10^8$ m/s. They are called pseudoranges to account for various errors such as synchronization offsets between the satellite and receiver clocks or additional delays due to the propagation of the GPS signal through the ionosphere and troposphere. Let $\boldsymbol{Y}_t$ be the observation vector at time t which is composed of the pseudoranges associated to the satellites tracked by the receiver (denoted hereafter SV for satellite in view). In the following, the subscript t refers to the t^{th} time step. We denote as n_t the dimension of this vector which can vary over time as a function of the relative geometry of the receiver and satellites. The k^{th} component of $\boldsymbol{Y}_t$, for $k = 1, \ldots, n_y$ takes the form

$$\boldsymbol{Y}_t(k) = \|\boldsymbol{p}_t - \boldsymbol{p}_t^k\| + b_t + \sqrt{\boldsymbol{\phi}_t(k)}\boldsymbol{w}_t(k) \qquad (1)$$

where,

- $\boldsymbol{p}_t = [x_t, y_t, z_t]^T$ represents the 3 position coordinates of the mobile in the system of coordinates chosen as a reference for the motion, here the Earth Centered Earth Fixed (ECEF)[1] frame,
- $\boldsymbol{p}_t^k = \left[x_t^k, y_t^k, z_t^k\right]^T$ is composed of the position coordinates of the k^{th} satellite,
- b_t is the GPS receiver clock offset with respect to the GPS reference time[2],
- $\boldsymbol{w}_t(k)$ is a white Gaussian random variable (RV) with variance unity,
- $\boldsymbol{\phi}_t = [\boldsymbol{\phi}_t(1), \ldots, \boldsymbol{\phi}_t(n_y)]$ is a vector composed of the variances of the measurement noise.

It should be noted that only the receiver clock offset is estimated since the satellite drift with respect to GPS time is usually well-modelled and compensated. Thus, the problem at hand is to estimate the position $\boldsymbol{p}_t$ and the observation noise variance $\boldsymbol{\phi}_t$ from the set of collected measurements $\boldsymbol{Y}_{1:l} = \{\boldsymbol{Y}_1, \ldots, \boldsymbol{Y}_l\}$ with possibly $l \geq t$. This paper assumes that the value of a pseudorange noise variance directly depends on the absence/presence of interferences affecting the measurement. Either they evolve slowly or they change abruptly under the influence of a nearby parasite RF emitter. To apply a Bayesian approach, *prior* stochastic models describing the dynamics of the unknown GPS navigation parameters are required. They are described in the next section.

III. BAYESIAN MODELING

This section describes the dynamic models assigned to the unknown parameters. In addition to estimating the dynamics of the mobile and the variance of the observation noise, a discrete-valued latent process $\{\boldsymbol{\lambda}_t\}_{t\geq 0}$ indicating the presence of variance jumps is introduced. More precisely, each component of this vector is associated with one of the pseudorange measurements collected at the current time t. A straightforward approach then consists of assigning two possible values to its components: one value indicating an abrupt change in the noise variance and the other value standing for a slow variance variation. However, we consider herein a more refined model taking into account *prior* knowledge of the GPS nominal performance level. Assuming no interference and no multipath, the variance of the GPS measurement noise can be approximately determined as a function of the class of the GPS receiver and the constellation geometry with respect to the mobile such as the satellite elevation angles. Recommendations of the radio technical commission for aeronautics (RTCA) to obtain the one-sigma GPS pseudorange error are given in [1]. To take advantage of this information, we adopt the following

[1]The ECEF system of coordinates is centered at the mass center of the earth, hence the name Earth-Centered. The z-axis is defined as being parallel to the earth rotational axes, pointing towards north. The x-axis intersects the sphere of the earth at the Greenwhich meridian and the y-axis lies in the equatorial plane.

[2]the GPS reference time is monitored by a set of clocks at the US naval observatory

definition for the k^{th} component ($k = 1, \ldots, n_y$) of vector $\boldsymbol{\lambda}_t$[3]

- $\boldsymbol{\lambda}_t(k) = 0$ if there is no variance jump on the k^{th} pseudorange at time t, i.e., if $\boldsymbol{\phi}_t(k)$ and $\boldsymbol{\phi}_{t-1}(k)$ take close values,
- $\boldsymbol{\lambda}_t(k) = 1$ if there is a variance jump due to interferences on the k^{th} pseudorange at time t,
- $\boldsymbol{\lambda}_t(k) = 2$ if there is a variance jump coinciding with the disappearance of all interference sources at time t.

Further on, we denote as $\Lambda = \left\{\boldsymbol{\Lambda}^j\right\}_{j=1,\ldots,n_\Lambda}$ the set of possible values for the indicator vector, whose cardinal is $n_\Lambda = 3^{n_y}$.

A. Motion model

The choice of the motion model depends on the dynamics of the mobile equipped with the GPS receiver. Classical models assume that one of the derivatives of the position coordinates, such as the acceleration or the jerk, is zero on average, hence can be represented as a white noise with a given variance. The reader interested in the derivation of such models is referred to [19]. We consider herein a 2nd-order model corresponding to a velocity on average uniform with occasional bursts of acceleration. In this case, the velocity $\dot{\boldsymbol{p}}_t$ of the mobile needs to be estimated jointly with its position and the resulting model is

$$\begin{pmatrix} \boldsymbol{p}_t \\ \dot{\boldsymbol{p}}_t \end{pmatrix} = \underbrace{\begin{pmatrix} \mathrm{I}_3 & T \times \mathrm{I}_3 \\ \mathbf{0}_3 & \mathrm{I}_3 \end{pmatrix}}_{F^p} \begin{pmatrix} \boldsymbol{p}_{t-1} \\ \dot{\boldsymbol{p}}_{t-1} \end{pmatrix} + \underbrace{\begin{pmatrix} \frac{\sigma_v T^2}{2} \times \mathrm{I}_3 \\ \sigma_v T \times \mathrm{I}_3 \end{pmatrix}}_{B^p} \boldsymbol{v}_t^p \quad (2)$$

where $\boldsymbol{v}_t^p$ is a unit variance white Gaussian noise, T is the time interval between two consecutive GPS measurements (classically 1 s) and σ_v is the standard deviation of the mobile acceleration.

B. Receiver clock model

The GPS receiver clock is a crystal oscillator which is not very accurate compared to satellite clocks. Usually, the evolution of its error with respect to GPS time is described by a 2nd order model representing both the clock bias and drift (corresponding to the phase and frequency error respectively) by random walks. Let b_t and d_t denote the bias and the drift at time t, respectively. They satisfy the following equation

$$\begin{pmatrix} b_t \\ d_t \end{pmatrix} = \underbrace{\begin{pmatrix} 1 & T \\ 0 & 1 \end{pmatrix}}_{F^c} \begin{pmatrix} b_{t-1} \\ d_{t-1} \end{pmatrix} + \boldsymbol{v}_t^c. \quad (3)$$

In this equation, $\boldsymbol{v}_t^c$ is a white Gaussian noise such that

$$\mathrm{E}\left[\boldsymbol{v}_t^c (\boldsymbol{v}_t^c)^T\right] = \underbrace{\begin{pmatrix} S_b T + S_d \frac{T^3}{3} & S_d \frac{T^2}{2} \\ S_d \frac{T^2}{2} & S_d T \end{pmatrix}}_{Q^c} \quad (4)$$

[3]A similar Markovian model with two possible states was introduced in [21] for detecting LOS and NLOS events for the localization of mobile terminals. However, the proposed three state Markovian model allows a finest description of interference effects in GPS navigation.

where the variances S_b and S_d are related to the Allan variance parameters as presented in [8]. Let $\boldsymbol{x}_t = \left[\boldsymbol{p}_t^T, \dot{\boldsymbol{p}}_t^T, b_t, d_t\right]^T$ stands for the state vector containing the mobile motion parameters. We denote as n_x the dimension of this state vector. From a probabilistic point of view, (2) and (4) are equivalent to

$$p\left(\boldsymbol{x}_t | \boldsymbol{x}_{t-1}\right) = \mathcal{N}\left(\boldsymbol{x}_t; F\boldsymbol{x}_{t-1}, Q\right) \quad (5)$$

where $\mathcal{N}\left(\boldsymbol{x}_t; F\boldsymbol{x}_{t-1}, Q\right)$ denotes a Gaussian density of argument $\boldsymbol{x}_t$, mean $F\boldsymbol{x}_{t-1}$ and covariance matrix Q. The matrices F and Q are block-diagonal matrices such that $F_t = \mathrm{diag}(F^p, F^c)$ and $Q_t = \mathrm{diag}(B^p (B^p)^T, Q^c)$, with $(B^p)^T$ the transpose of B^p.

By introducing the state vector, the observation equation (1) can be rewritten

$$\boldsymbol{Y}_t(k) = \boldsymbol{h}_t^k(\boldsymbol{x}_t) + \sqrt{\boldsymbol{\phi}_t(k)}\boldsymbol{w}_t(k) \quad (6)$$

where

$$\boldsymbol{h}_t^k(\boldsymbol{x}_t) = \|\boldsymbol{p}_t - \boldsymbol{p}_t^k\| + b_t \quad (7)$$

C. Variance model

In the same manner as in [3] and [23], we assign a conjugate inverse gamma ($\mathcal{IG}$) *prior* to the components of the variance vector $\boldsymbol{\phi}_t$

$$\boldsymbol{\phi}_t(k) | \boldsymbol{\phi}_{t-1}(k), \boldsymbol{\lambda}_t(k) \sim \mathcal{IG}\left(\boldsymbol{\phi}_t(k); \alpha\left(\boldsymbol{\lambda}_t(k)\right), \beta\left(\boldsymbol{\lambda}_t(k)\right)\right) \quad (8)$$

where

$$\mathcal{IG}\left(x; a, b\right) = \frac{b^a}{\Gamma(a)} x^{-a-1} \exp\left(-\frac{b}{x}\right) \mathcal{I}_{\mathbb{R}^+}(x) \quad (9)$$

with $\Gamma(.)$ the Gamma function and $\mathcal{I}_{\mathbb{R}^+}(x)$ the indicator function on $\mathbb{R}^+$. Using an $\mathcal{IG}$ *prior* is a convenient choice since it is the conjugate distribution of the variance of a Gaussian distribution. In other words, in a Bayesian setting, whenever an $\mathcal{IG}$ *prior* is selected for the variance, the corresponding *posterior* distribution is also an Inverse-Gamma distribution. In the sequel, this property makes it easier to define efficient proposal distributions for the navigation states and variance parameters. The values of the hyperparameters $\alpha\left(\boldsymbol{\lambda}_t(k)\right)$ and $\beta\left(\boldsymbol{\lambda}_t(k)\right)$ are adjusted as a function of $\boldsymbol{\lambda}_t(k)$ to enforce the following characteristics for the $\mathcal{IG}$ distribution.

- Case 1 ($\boldsymbol{\lambda}_t(k) = 0$): the $\mathcal{IG}$ distribution has a small standard deviation $\sigma_0^{\mathcal{IG}}$ and a mean $\mu_0^{\mathcal{IG}}$ equal to $\boldsymbol{\phi}_{t-1}(k)$. Thus, we set
$$\begin{aligned} \alpha(0) &= (\mu_0^{\mathcal{IG}}/\sigma_0^{\mathcal{IG}})^2 + 2 \\ \beta(0) &= \mu_0^{\mathcal{IG}}(\alpha(0) - 1). \end{aligned}$$
- Case 2 ($\boldsymbol{\lambda}_t(k) = 1$): the $\mathcal{IG}$ distribution is heavy-tailed with a first inflection point slightly higher than the nominal value of the GPS noise variance and a second inflection point set to the maximal value before the receiver loss of lock. Let $I_{\min}$ and $I_{\max}$ denote the smaller and the higher inflection points of the $\mathcal{IG}$ distribution. By denoting $r = I_{\min}/I_{\max}$, we obtain the following definition for the $\mathcal{IG}$ parameters
$$\begin{aligned} \alpha(1) &= \left((r+1)/(r-1)\right)^2 \\ \beta(1) &= 2I_{\max} r(r+1)/(r-1)^2. \end{aligned}$$

- Case 3 ($\boldsymbol{\lambda}_t(k) = 2$): the $\mathcal{IG}$ distribution is peaky with a mean $\mu_2^{\mathcal{IG}}$ equal to the nominal value of the GPS observation noise variance and a very small standard deviation $\sigma_2^{\mathcal{IG}}$. Therefore, as for case 1, the $\mathcal{IG}$ parameters are set to

$$\begin{aligned} \alpha(2) &= (\mu_2^{\mathcal{IG}}/\sigma_2^{\mathcal{IG}})^2 + 2 \\ \beta(2) &= \mu_2^{\mathcal{IG}}(\alpha(2) - 1). \end{aligned}$$

The exact values of the means, standard deviations and inflection points of these $\mathcal{IG}$ distributions are provided in section V.

D. Indicator prior

The components of the vector $\boldsymbol{\lambda}_t$ are assumed *a priori* independent and have the following discrete distribution

$$P\left[\boldsymbol{\lambda}_t(k) = 0 | \boldsymbol{\lambda}_{0:t-1}(k)\right] = 1 - \gamma \quad (10)$$

$$P\left[\boldsymbol{\lambda}_t(k) = 1 | \boldsymbol{\lambda}_{0:t-1}(k)\right] = \gamma \mu_t(k) \quad (11)$$

$$P\left[\boldsymbol{\lambda}_t(k) = 2 | \boldsymbol{\lambda}_{0:t-1}(k)\right] = \gamma \left(1 - \mu_t(k)\right) \quad (12)$$

where γ is the probability that a variance jump occurs and $\mu_t(k)$ is the probability that this variance jump coincides with interferences. The probability γ is set *a priori* whereas the value of $\mu_t(k)$ varies depending whether the k^{th} pseudorange is corrupted by interferences or not. More precisely, in the absence of interferences, the only possibility is an increase in variance ($\mu_t(k) = 1$). On the contrary, in the presence of interferences, either they can disappear or the variance can switch to a different value if the RF environment changes ($\mu_t(k) = 0.5$). To adjust the probability $\mu_t(k)$, we introduce additional Bernoulli random variables $\{\boldsymbol{\epsilon}_t(k)\}_{k=1,\ldots,n_t}$ which satisfy

$$\boldsymbol{\epsilon}_t(k) = 1 \text{ in the presence of interferences} \quad (13)$$

$$\boldsymbol{\epsilon}_t(k) = 0 \text{ otherwise.} \quad (14)$$

These Bernoulli random variables evolve with the vector $\boldsymbol{\lambda}_t$ as follows

$$\boldsymbol{\epsilon}_t(k) = \begin{cases} \boldsymbol{\epsilon}_{t-1}(k) & \text{if } \boldsymbol{\lambda}_t(k) = 0 \\ 1 & \text{if } \boldsymbol{\lambda}_t(k) = 1 \\ 0 & \text{if } \boldsymbol{\lambda}_t(k) = 2. \end{cases} \quad (15)$$

The probability $\mu_t(k)$ is finally defined as

$$\mu_t(k) = \begin{cases} 1 & \text{if } \boldsymbol{\epsilon}_{t-1}(k) = 0 \\ 0.5 & \text{otherwise.} \end{cases} \quad (16)$$

It should be noted that the way the value of $\mu_t(k)$ is selected makes $\boldsymbol{\lambda}_t(k)$ dependent on $\boldsymbol{\lambda}_{0:t-1}(k)$, hence the expression of the transition probabilities in equations (10)-(12).

The Bayesian model defined in this section is summarized in Fig.1 which presents the relationships between the different unknown parameters. The evolution of the navigation and variance states $\boldsymbol{X}_t$ depends on the indicator vector $\boldsymbol{\lambda}_t$ which also evolves. The discrete-valued vector $\boldsymbol{\epsilon}_t$ is used to finely tune the *prior* distribution of $\boldsymbol{\lambda}_t$. The aim of the algorithm developed in the next section is to estimate accurately the hidden state $\boldsymbol{X}_t$ from the GPS measurements $\boldsymbol{Y}_t$ even though the variance noise may be switching.

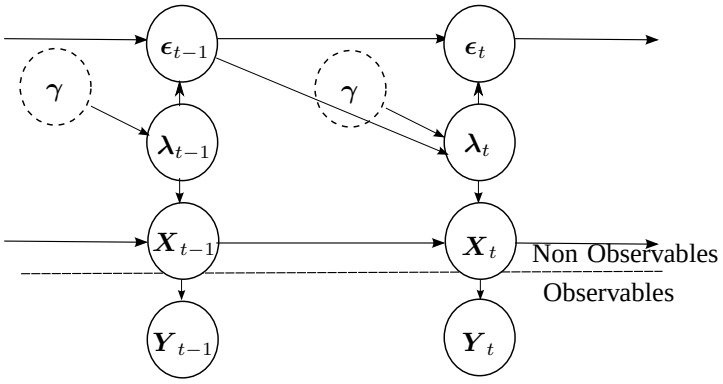

Fig. 1. Directed Acyclic Graph (DAG) illustrating the dependencies between the model parameters and the GPS observations. The fixed parameters appear as dashed boxes.

IV. Fixed-lag particle smoother

In order to mitigate interferences in GPS navigation, we propose to estimate jointly the discrete-valued indicator vector $\boldsymbol{\lambda}_t$ and continuous-valued parameters such as the mobile motion states and the observation noise variance, i.e. estimate $\boldsymbol{X}_t = [\boldsymbol{x}_t^T, \boldsymbol{\phi}_t^T]^T$. In a Bayesian framework, all inference is based on the *posterior* distribution of the unknown parameters given the set of available observations, expressed as $p\left(\boldsymbol{S}_{0:t} | \boldsymbol{Y}_{1:t}\right)$ with $\boldsymbol{S}_t = \left[\boldsymbol{X}_t^T, \boldsymbol{\lambda}_t^T\right]^T$ and $\boldsymbol{S}_{0:t} = (\boldsymbol{S}_0, \ldots, \boldsymbol{S}_t)$. PFs are a class of methods well-suited to perform the estimation of the hybrid state vector $\boldsymbol{S}_{0:t}$. They approximate the target distribution by an empirical distribution

$$\widehat{p}\left(\boldsymbol{S}_{0:t} | \boldsymbol{Y}_{1:t}\right) = \sum_{i=1}^{N} w_t^i \delta\left(\boldsymbol{S}_{0:t} - \boldsymbol{S}_{0:t}^i\right), \quad \sum_{i=1}^{N} w_t^i = 1 \quad (17)$$

where δ is the Dirac delta function. The weights w_t^i and the N support points $\boldsymbol{S}_{0:t}^i$ (referred to as particles) are classically obtained by applying sequentially the importance sampling (IS) technique. Ideally, the particles should be sampled directly from the target distribution $p\left(\boldsymbol{S}_{0:t} | \boldsymbol{Y}_{1:t}\right)$, and assigned equal weights. Since it is usually impossible to sample $p\left(\boldsymbol{S}_{0:t} | \boldsymbol{Y}_{1:t}\right)$, they are drawn instead from a proposal distribution $\pi\left(\boldsymbol{S}_{0:t} | \boldsymbol{Y}_{1:t}\right)$, called importance distribution [4] [16]. Then, the weights are used to correct the discrepancy between p and π

$$w_t^i \propto \frac{p\left(\boldsymbol{S}_{0:t}^i | \boldsymbol{Y}_{1:t}\right)}{\pi\left(\boldsymbol{S}_{0:t}^i | \boldsymbol{Y}_{1:t}\right)} \quad (18)$$

where '$\propto$' means 'proportional to'. A sequential formulation of IS allows one to leave the previous particles $\boldsymbol{S}_{0:t-1}^i$ unchanged by only simulating at time step t

$$\boldsymbol{S}_t^i \sim \pi\left(\boldsymbol{S}_t | \boldsymbol{S}_{0:t-1}^i, \boldsymbol{Y}_{1:t}\right). \quad (19)$$

Then, the importance weights can be updated using

$$w_t^i \propto w_{t-1}^i \frac{p\left(\boldsymbol{Y}_t | \boldsymbol{S}_t^i\right) p\left(\boldsymbol{S}_t^i | \boldsymbol{S}_{0:t-1}^i\right)}{\pi\left(\boldsymbol{S}_t^i | \boldsymbol{S}_{0:t-1}^i, \boldsymbol{Y}_{1:t}\right)}. \quad (20)$$

Unfortunately, these algorithms are known to experience degeneracy issues so that after a few iterations, all but one particle have negligible normalized weights. To overcome

this inherent limitation, a selection step is introduced which consists of resampling the set of particles according to the estimated empirical distribution. The reader is invited to consult [14] for more details.

A. Estimation objectives

Several realizations are necessary to obtain a good estimation of the variance of a stochastic process, hence we propose to use near future measurements to detect and estimate the variance jumps. The so-called fixed lag PF (FLPF) aims at estimating a time t the distribution $p\left(\boldsymbol{S}_{0:t}|\boldsymbol{Y}_{1:t+L}\right)$, with a lag $L>0$. For that purpose, we first compute an approximation of the smoothing distribution

$$\widehat{p}\left(\boldsymbol{S}_{0:t+L}|\boldsymbol{Y}_{1:t+L}\right)=\sum_{i=1}^{N}w_{t+L}^{i}\delta\left(\boldsymbol{S}_{0:t+L}-\boldsymbol{S}_{0:t+L}^{i}\right). \quad (21)$$

The distribution of interest is then obtained by marginalization

$$\widehat{p}\left(\boldsymbol{S}_{0:t}|\boldsymbol{Y}_{1:t+L}\right)=\sum_{i=1}^{N}w_{t+L}^{i}\delta\left(\boldsymbol{S}_{0:t}-\boldsymbol{S}_{0:t}^{i}\right). \quad (22)$$

The estimation of the parameters of interest is achieved as follows

$$\mathrm{E}\left[\boldsymbol{X}_{t}|\boldsymbol{Y}_{1:t+L}\right]\simeq\sum_{i=1}^{N}w_{t+L}^{i}\boldsymbol{X}_{t}^{i}. \quad (23)$$

Finally, the detection of a variance jump affecting the k^{th} pseudorange is based on the posterior change probability

$$\begin{aligned}P_{t}^{k} &= P\left[\boldsymbol{\lambda}_{t}(k)\neq 0|\boldsymbol{Y}_{1:t+L}\right]\\ &\simeq \sum_{i=1}^{N}w_{t+L}^{i}\left[1-\delta\left(\boldsymbol{\lambda}_{t}^{i}(k)\right)\right]. \end{aligned} \quad (24)$$

B. Particle propagation strategy

It is well-known that the choice of the importance distribution is a critical issue to design efficient PF algorithms. To generate samples in interesting regions of the state space, i.e., corresponding to a high likelihood $p\left(\boldsymbol{Y}_{t}|\boldsymbol{S}_{t}\right)$, a natural strategy consists of taking into account information from the most recent observations. Thus, the optimal importance distribution in the sense that it minimizes the variance of the importance weights has been introduced in [33]

$$\pi\left(\boldsymbol{S}_{t}|\boldsymbol{S}_{0:t-1}^{i},\boldsymbol{Y}_{t}\right)=p\left(\boldsymbol{S}_{t}|\boldsymbol{S}_{0:t-1}^{i},\boldsymbol{Y}_{t}\right). \quad (25)$$

However, this distribution is usually analytically intractable and sub-optimal approximations based on extended Kalman filter [4] or more recently unscented Kalman filter [10] schemes are used. The problem at hand requires sampling from a high-dimensional state space $\mathbb{R}^{n_x}\times\mathbb{R}^{n_t}\times n_\Lambda$ involving both discrete-valued and continuous-valued parameters. In this context, an efficient sampling scheme consisting of simulating the continuous states while exploring exhaustively the possible values of the discrete states was proposed in [22]. Assume at time $t-1$ the following approximation of the target distribution is available

$$\widehat{p}(\boldsymbol{S}_{0:t-1}|\boldsymbol{Y}_{1:t-1})=\sum_{i=1}^{N}w_{t-1}^{i}\delta\left(\boldsymbol{S}_{0:t-1}-\boldsymbol{S}_{0:t-1}^{i}\right). \quad (26)$$

Then, a combination of deterministic and random propagation schemes yields at time t

$$\widehat{p}\left(\boldsymbol{S}_{0:t}\ |\boldsymbol{Y}_{1:t}\right)= \quad (27)$$
$$\sum_{j=1}^{n_\Lambda}\sum_{i=1}^{N}w_{t}^{i,j}\delta\left(\boldsymbol{S}_{0:t}-\left\{\boldsymbol{S}_{0:t-1}^{i},\underbrace{\boldsymbol{X}_{t}^{i,j},\boldsymbol{\lambda}_{t}^{i,j}=\boldsymbol{\Lambda}^{j}}_{\boldsymbol{S}_{t}^{i,j}}\right\}\right).$$

where the discrete-valued part of $\boldsymbol{S}_{t}^{i,j}$, i.e., $\boldsymbol{\lambda}_{t}^{i,j}$, is the j^{th} element of the set Λ and the continuous-valued part $\boldsymbol{X}_{t}^{i,j}$ is drawn from an importance distribution $\pi\left(\boldsymbol{X}_{t}|\boldsymbol{S}_{t-1}^{i},\boldsymbol{\lambda}_{t}^{i,j}=\boldsymbol{\Lambda}^{j},\boldsymbol{Y}_{t}\right)$ whose choice is discussed later. The importance weights $w_{t}^{i,j}$ are equal to

$$w_{t}^{i,j}=\frac{p\left(\boldsymbol{S}_{0:t}^{i,j}|\boldsymbol{Y}_{1:t}\right)}{\pi\left(\boldsymbol{X}_{0:t}^{i,j}|\boldsymbol{\lambda}_{0:t}^{i,j},\boldsymbol{Y}_{1:t}\right)}. \quad (28)$$

From Bayes'rule, we obtain

$$\begin{aligned}p\left(\boldsymbol{S}_{0:t}^{i,j}|\boldsymbol{Y}_{1:t}\right)\propto\ & p\left(\boldsymbol{Y}_{t}|\boldsymbol{X}_{t}^{i,j}\right)p\left(\boldsymbol{X}_{t}^{i,j}|\boldsymbol{\lambda}_{t}^{i,j}=\boldsymbol{\Lambda}^{j},\boldsymbol{S}_{t-1}^{i}\right)\\ &\times P\left[\boldsymbol{\lambda}_{t}^{i,j}=\boldsymbol{\Lambda}^{j}|\boldsymbol{\lambda}_{0:t-1}^{i}\right]p\left(\boldsymbol{S}_{0:t-1}^{i,j}|\boldsymbol{Y}_{1:t-1}\right). \end{aligned} \quad (29)$$

In addition, the considered importance distribution can be decomposed in the following manner

$$\begin{aligned}\pi\left(\boldsymbol{X}_{0:t}^{i,j}|\boldsymbol{\lambda}_{0:t}^{i,j},\boldsymbol{Y}_{1:t}\right)\propto\ & \pi\left(\boldsymbol{X}_{t}^{i,j}|\boldsymbol{S}_{t-1}^{i},\boldsymbol{\lambda}_{t}^{i,j},\boldsymbol{Y}_{t}\right)\\ &\times\pi\left(\boldsymbol{X}_{0:t-1}^{i,j}|\boldsymbol{\lambda}_{0:t-1}^{i,j},\boldsymbol{Y}_{1:t-1}\right). \end{aligned} \quad (30)$$

Thus, by combining (29) and (30), the weights appearing in (27) are equal to

$$w_{t}^{i,j}\propto K_{t}^{i,j}P\left[\boldsymbol{\lambda}_{t}=\boldsymbol{\Lambda}^{j}|\boldsymbol{\lambda}_{0:t-1}^{i}\right]w_{t-1}^{i} \quad (31)$$

where

$$K_{t}^{i,j}=\frac{p\left(\boldsymbol{Y}_{t}|\boldsymbol{X}_{t}^{i,j}\right)p\left(\boldsymbol{X}_{t}^{i,j}|\boldsymbol{\lambda}_{t}^{i,j}=\boldsymbol{\Lambda}^{j},\boldsymbol{S}_{t-1}^{i}\right)}{\pi\left(\boldsymbol{X}_{t}^{i,j}|\boldsymbol{S}_{t-1}^{i},\boldsymbol{\lambda}_{t}=\boldsymbol{\Lambda}^{j},\boldsymbol{Y}_{t}\right)}. \quad (32)$$

When using a fixed-lag PF to enhance variance jump detection, the deterministic approach proposed in [22] can be extended to obtain the approximated smoothing distribution

$$\widehat{p}\left(\boldsymbol{S}_{0:t+L}|\boldsymbol{Y}_{1:t+L}\right)= \quad (33)$$
$$\sum_{J\in S_{J}}\sum_{i=1}^{N}w_{t+L}^{i,J}\delta\left(\boldsymbol{S}_{0:t+L}-\left\{\boldsymbol{S}_{0:t-1}^{i},\boldsymbol{X}_{t:t+L}^{i,J},\boldsymbol{\lambda}_{t:t+L}^{i,J}=\boldsymbol{\Lambda}^{J}\right\}\right)$$

where S_J is the set of $(L+1)$-uplets $J=(j_0,\ldots,j_L)$ with $j_l\in\{0,\ldots,n_\Lambda-1\}$ referring to the j_l^{th} possible value of vector $\boldsymbol{\lambda}_t$. More precisely, $\boldsymbol{\Lambda}^{J}=\left(\boldsymbol{\Lambda}^{j_0},\ldots,\boldsymbol{\Lambda}^{j_1}\right)$. In this case, the smoothing weights are computed as

$$w_{t+L}^{i,J}\propto K_{t+L}^{i,J}P\left[\boldsymbol{\lambda}_{t:t+L}=\boldsymbol{\Lambda}^{J}|\boldsymbol{\lambda}_{0:t-1}^{i}\right]w_{t-1}^{i} \quad (34)$$

where

$$K_{t+L}^{i,J} = \frac{\prod_{l=0}^{L} p\left(\boldsymbol{Y}_{t+l}|\boldsymbol{X}_{t+l}^{i,J}\right) p\left(\boldsymbol{X}_{t+l}^{i,J}|\boldsymbol{S}_{t+l-1}^{i,J}, \boldsymbol{\lambda}_{t+l}^{i,J} = \boldsymbol{\Lambda}^{j_l}\right)}{\pi\left(\boldsymbol{X}_{t:t+L}^{i,J}|\boldsymbol{S}_{t-1}^{i}, \boldsymbol{\lambda}_{t:t+L} = \boldsymbol{\Lambda}^{J}, \boldsymbol{Y}_{t:t+L}\right)}. \quad (35)$$

The main advantage of this approach is that there is no risk to discard useful information as when drawing one particle out of the n_Λ possibilities for vector $\boldsymbol{\lambda}_t$. However, the gain in performance should be balanced with the increased computational complexity. Each particle at time $t-1$ results in n_λ^{L+1} offsprings (instead of one for usual PF implementations). After the propagation step, the total number of particles amounts to $N \times n_\lambda^{L+1}$, hence increases exponentially with the lag L. To keep the computational cost reasonable, we propose to limit the paths to consider for vector $\boldsymbol{\lambda}_t$ by taking advantage of the sparseness of variance jump events. When detecting variance jumps at time t, it can be assumed that no jump occurs during time interval $[t+1, t+L]$, which is *a priori* the most probable event. Therefore, the sum in equation (33) can be restricted to the sequences $\boldsymbol{\lambda}_{t:t+L}^{(j)} = \boldsymbol{\Lambda}_0^j$ where $\boldsymbol{\Lambda}_0^j = \left(\boldsymbol{\Lambda}^j, \mathbf{0}, \ldots, \mathbf{0}\right)$, with $j = 1, \ldots, n_\Lambda$, yielding to the following approximation

$$\widehat{p}\left(\boldsymbol{S}_{0:t+L}|\boldsymbol{Y}_{1:t+L}\right) = \sum_{j=1}^{n_\Lambda}\sum_{i=1}^{N} w_{t-1}^{i,j}\delta\left(\boldsymbol{S}_{0:t+L} - \left\{\boldsymbol{X}_{0:t-1}^{i}, \boldsymbol{X}_{t:t+L}^{i,j}, \boldsymbol{\lambda}_{t:t+L}^{i,j} = \boldsymbol{\Lambda}_0^j\right\}\right). \quad (36)$$

This strategy was proved to be efficient for multipath mitigation in [15]. Its consequences on the estimation of variance jumps are discussed in section IV dedicated to simulation results.

C. Proposal distribution for the continuous states

The uncertainty on the measurement noise variance after a jump imposes to select a non informative *prior* distribution as in section II. It is thus important to integrate information from the GPS measurements to sample relevant variance values. As discussed beforehand, the optimal proposal is given by

$$p\left(\boldsymbol{X}_{t:t+L}|\boldsymbol{X}_{t-1}^{i}, \boldsymbol{\lambda}_{t:t+L}^{i,j} = \boldsymbol{\Lambda}_0^j, \boldsymbol{Y}_{t:t+L}\right). \quad (37)$$

This distribution is non standard and cannot be sampled from efficiently. Thus we introduce a proposal distribution which is an approximation of (37) but still preserves information from the measurements. First, given the assumption that no variance jump occurs during time interval $[t+1, t+L]$, the variance can be considered constant during this period. Therefore, it is sufficient to simulate $\boldsymbol{\phi}_t$ and then set $\boldsymbol{\phi}_{t+l} = \boldsymbol{\phi}_t$ for $l = 1, \ldots, L$. Particle propagation can thus be performed in three steps.

1) Simulation of the mobile motion parameters,

$$\boldsymbol{x}_{t:t+L}^{i,j} \sim \pi\left(\boldsymbol{x}_{t:t+L}|\boldsymbol{X}_{t-1}^{i}, \boldsymbol{\lambda}_{t:t+L}^{i,j} = \boldsymbol{\Lambda}_0^j, \boldsymbol{Y}_{t:t+L}\right).$$

2) Simulation of the variance vector $\boldsymbol{\phi}_t$,

$$\boldsymbol{\phi}_t^{i,j} \sim \pi\left(\boldsymbol{\phi}_t|\boldsymbol{x}_{t:t+L}^{i,j}, \boldsymbol{X}_{t-1}^{i}, \boldsymbol{\lambda}_{t:t+L}^{i,j} = \boldsymbol{\Lambda}_0^j, \boldsymbol{Y}_{t:t+L}\right).$$

3) Extrapolation,

$$\boldsymbol{\phi}_{t+l}^{i,j} = \boldsymbol{\phi}_t^{i,j}, \text{ for } l = 1, \ldots, L.$$

The proposal distributions corresponding to steps 1) and 2) are described hereafter.

1) Variance parameter simulation: Using Bayes' rule, the optimal importance distribution for the variance parameters can be decomposed as

$$p(\boldsymbol{\phi}_t|\boldsymbol{x}_{t:t+L}^{i,j}, \boldsymbol{X}_{t-1}^{i}, \boldsymbol{\lambda}_{t:t+L}^{i,j} = \boldsymbol{\Lambda}_0^j, \boldsymbol{Y}_{t:t+L}) \propto p\left(\boldsymbol{Y}_{t:t+L}|\boldsymbol{x}_{t:t+L}^{i,j}, \boldsymbol{\phi}_t\right) p\left(\boldsymbol{\phi}_t|\boldsymbol{\phi}_{t-1}^{i}, \boldsymbol{\lambda}_t^{i,j} = \boldsymbol{\Lambda}^j\right). \quad (38)$$

The *prior* of the variance vector components is an $\mathcal{IG}$-distribution. In addition, seen as a function of vector $\boldsymbol{\phi}_t$, the likelihood function $p\left(\boldsymbol{Y}_{t:t+L}|\boldsymbol{x}_{t:t+L}^{i,j}, \boldsymbol{\phi}_t\right)$ takes the form of a product of $\mathcal{IG}$-distributions up to a proportional constant. It follows that the observation noise variances at time t can be generated independently as

$$\boldsymbol{\phi}_t^{i,j}(k) \sim \mathcal{IG}\left(\boldsymbol{\phi}_t(k); \tilde{\alpha}_t^{i,j}(k), \tilde{\beta}_t^{i,j}(k)\right) \quad (39)$$

where the $\mathcal{IG}$ parameters are given by

$$\tilde{\alpha}_t^{i,j}(k) = \alpha\left(\boldsymbol{\Lambda}^j(k)\right) + (L+1)/2 \quad (40)$$

$$\tilde{\beta}_t^{i,j}(k) = \beta\left(\boldsymbol{\Lambda}^j(k)\right) + \Delta\beta_t^{i,j}(k). \quad (41)$$

In (41), the increment in the *prior* value of parameter β, denoted above $\Delta\beta_t^{i,j}(k)$, is equal, up to a proportionality constant, to the estimation of the measurement noise variance from $L+1$ consecutive observations

$$\Delta\beta_t^{i,j}(k) = \frac{1}{2}\sum_{l=0}^{L+1}\left(\boldsymbol{Y}_{t+l}(k) - \boldsymbol{h}_{t+l}^{k}\left(\boldsymbol{x}_{t+l}^{i,j}\right)\right)^2. \quad (42)$$

2) Motion parameter simulation: The proposal distribution for the motion parameters can theoretically be obtained by marginalizing the joint distribution of the continuous states

$$p(\boldsymbol{x}_{t:t+L}|\boldsymbol{X}_{t-1}^{i}, \boldsymbol{\lambda}_{t:t+L} = \boldsymbol{\Lambda}_0^j, \boldsymbol{Y}_{t:t+L}) = \int_{\boldsymbol{\phi}_t} p\left(\boldsymbol{x}_{t:t+L}, \boldsymbol{\phi}_t|\boldsymbol{X}_{t-1}^{i}, \boldsymbol{\lambda}_{t:t+L} = \boldsymbol{\Lambda}_0^j, \boldsymbol{Y}_{t:t+L}\right) d\boldsymbol{\phi}_t. \quad (43)$$

Using Bayes' rule to compute (43), the following result can be obtained

$$p(\boldsymbol{x}_{t:t+L}|\boldsymbol{X}_{t-1}^{i}, \boldsymbol{\lambda}_{t:t+L} = \boldsymbol{\Lambda}_0^j, \boldsymbol{Y}_{t:t+L}) \propto p\left(\boldsymbol{x}_{t:t+L}|\boldsymbol{x}_{t-1}^{i}\right)\prod_{k=1}^{n_y}\left(\tilde{\beta}_t^{i,j}(k)\right)^{-\tilde{\alpha}_t^{i,j}(k)}. \quad (44)$$

This distribution is not easy to simulate. However, an accurate Gaussian approximation can be used instead as detailed in appendix A. Using this approximation, we simulate the motion vectors, for $l = 0, \ldots, L$, according to

$$p(\boldsymbol{x}_{t+l}|\boldsymbol{x}_{t+l-1}^{i,j}, \boldsymbol{\lambda}_t = \boldsymbol{\Lambda}^j, \boldsymbol{Y}_{t:t+l}) \simeq \mathcal{N}(\boldsymbol{x}_{t+l}; \boldsymbol{m}_{t+l}^{i,j}, \Sigma_{t+l}^{i,j})$$

where

$$\Sigma_{t+l}^{i,j} = \left(\left(H_{t+l}^{i,j}\right)^T\left(D_t^{i,j}\right)^{-1}H_{t+l}^{i,j} + Q\right)^{-1}$$

$$\boldsymbol{m}_{t+l}^{i,j} = \Sigma_{t+l}^{i,j}\left(Q^{-1}F\boldsymbol{x}_{t+l-1}^{i,j} + \left(D_t^{i,j}\right)^{-1}\left(H_{t+l}^{i,j}\right)^T\Delta\boldsymbol{Y}_{t+l}^{i,j}\right).$$

In these equations, $H_{t+l}^{i,j}$ is the matrix of the partial derivatives of vectorial function $\boldsymbol{h}_{t+l}$ evaluated in $\boldsymbol{x}_{t+l} = F\boldsymbol{x}_{t+l-1}^{i,j}$. Furthermore,

$$D_t^{i,j} = \text{diag}\left(\boldsymbol{V}_t^{i,j}\right) \tag{45}$$

with the components of the vector $\boldsymbol{V}_t^{i,j}$ defined as

$$\boldsymbol{V}_t^{i,j}(k) = \beta(\boldsymbol{\Lambda}^j(k))\left(\alpha(\boldsymbol{\Lambda}^j(k)) + L/2\right)^{-1}. \tag{46}$$

Finally, we have

$$\Delta\boldsymbol{Y}_{t+l}^{i,j} = \boldsymbol{Y}_{t+l} - \boldsymbol{h}_{t+l}(F\boldsymbol{x}_{t+l-1}^{i,j}) + H_{t+l}^{i,j}F\boldsymbol{x}_{t+l-1}^{i,j}. \tag{47}$$

D. Algorithmic enhancements

1) Hypothesis test: After the propagation step, the number of particles in the FLPF is multiplied by n_Λ^{L+1}. Therefore, a selection procedure has to be used to keep the number of particles constant. Two different approaches can be applied. The simplest one consists of selecting the N best particles among the $N \times n_\Lambda^{L+1}$ ones. As an alternative, sampling with replacement according to the smoothing weights $w_{t+L}^{i,j}$ could be employed. A more efficient strategy is proposed here. Indeed, estimating the variance of a stochastic process is a challenging issue when the number of available realizations is limited. In our case, if L is small, the detection of a variance jump may not be clear cut. Thus, it may take a few time steps before the majority of the particles indicate the presence of interferences. The longer it takes, the larger the position estimation error. To bypass this limitation and thereby improve the tracking ability of our algorithm, we propose to help particle selection by applying a hypothesis test with the following hypotheses

- H_t^0: no variance jump,
- H_t^1: variance jump.

According to Bayesian decision theory, hypothesis H_t^1 is accepted if the following inequality is satisfied

$$\frac{P\left[H_t^1|\boldsymbol{Y}_{1:t+L}\right]}{P\left[H_t^0|\boldsymbol{Y}_{1:t+L}\right]} \geq T_h \tag{48}$$

where T_h is a threshold depending on the probability of false alarm of the test. The *posterior* probabilities $P\left[H_t^i|\boldsymbol{Y}_{1:t+L}\right]$, for $i = \{0,1\}$, can be directly approximated from the PF smoothing weights

$$P\left[H_t^0|\boldsymbol{Y}_{1:t+L}\right] \simeq \sum_{i=1}^{N}\sum_{j=1}^{n_\lambda} w_{t+L}^{i,j}\delta(\boldsymbol{\lambda}_t^{i,j}) \tag{49}$$

$$P\left[H_t^1|\boldsymbol{Y}_{1:t+L}\right] = 1 - P\left[H_t^0|\boldsymbol{Y}_{1:t+L}\right]. \tag{50}$$

At that stage, the most straightforward use of the statistic test resulting from (48) consists of discarding all the particles standing for the wrong hypothesis. However, the convergence properties of the PF would be lost. We propose a more flexible strategy allowing the algorithm to recover from a wrong decision. The idea is to resample the particles according to auxiliary weights as advocated in [20]. These resampling weights are derived from the smoothing weights by penalizing irrelevant particles whenever a variance jump is detected as follows

$$\alpha_t^{i,j} \propto \left(w_{t+L}^{i,j}\right)^\beta, \text{ if } \boldsymbol{\lambda}_t^{i,j} = \boldsymbol{0} \tag{51}$$

$$\alpha_t^{i,j} \propto w_{t+L}^{i,j} \text{ otherwise.} \tag{52}$$

In expression (51), β is a penalizing factor ($\beta > 1$). Then, the resampling is performed in two steps. First, N particles are sampled with replacement out of the $N \times n_\Lambda$ according the auxiliary weights $\alpha_t^{i,j}$. Unfortunately, the generated particles are not distributed anymore according to an approximation of the filtering distribution $p\left(\boldsymbol{S}_{0:t}|\boldsymbol{Y}_{1:t}\right)$ as required to proceed to next step of the PF. Hence, they are assigned new weights to remedy this problem. Thus, the proposed resampling procedure is the following.

For $l = 1, \ldots, N$, a new particle $\boldsymbol{S}_t^l$ is drawn out of the $N \times n_\Lambda$ particles $\boldsymbol{S}_t^{i,j}$ ($i = 1, \ldots, N$ and $j = 1, \ldots, n_\Lambda$) according to the multinomial distribution with probabilities $\alpha_t^{i,j}$. Then, assuming vector $\boldsymbol{S}_t^{p,q}$ is selected, the particle is assigned the weight $w_t^l \propto w_t^{p,q}/\alpha_t^{p,q}$ to make sure an approximation of $p\left(\boldsymbol{S}_{0:t}|\boldsymbol{Y}_{1:t}\right)$ is obtained before proceeding to the next iteration.

In this way, the variability of PF weights is artificially reduced by enforcing the removal of the particles that are less likely to survive at the next time steps. Furthermore, detection of small variance jumps and estimation of their amplitudes is improved even with a small lag L and a reasonable number of particles.

2) Dynamic prior probabilities: This section presents an extension of the proposed FLPF which aims at preventing false detections of variance jumps which can severely impair the estimation of the mobile motion parameters. In section III, the vectors $\boldsymbol{\lambda}_t$ are assumed time-independent for the sake of simplicity. However, as already pointed out in the work of De Cambry [9] dedicated to the off-line segmentation of stochastic signals, this assumption can lead to close detections of changes in the signal model hence to an over-segmentation. To prevent false detections, De Cambry introduces a minimal duration constraint. Similarly, we could restrict the set of possible offsprings of the parent particles $\boldsymbol{\lambda}_{0:t-1}^i$ by enforcing a minimal delay between too consecutive variance jumps. Although this approach allows one to reduce the computational complexity, it turns out to be difficult to set the minimal delay. Indeed, it depends both on the mobile velocity and the number of interference sources in the navigation environment. As an alternative, we propose to adjust the value of the variance jump *prior* probability γ as a increasing function of the elapsed time since the last jump. More precisely, the following rule is adopted

$$\gamma_t^i(k) = \exp\left[\left(1 + \frac{1}{t - t_{occ}^i(k)}\right)\ln(\gamma_m)\right] \tag{53}$$

where the superscript i refers to the i^{th} particle, k corresponds to the k^{th} component of the observation vector and γ_m is the maximum value allowed for the probabilities $\gamma_t^i(k)$. Here $t_{occ}^i(k)$ is the last time particle i indicated a variance jump, that is

$$t_{occ}^i(k) = \max\left\{u \leq t|\boldsymbol{\lambda}_u^i(k) = 1\right\}. \tag{54}$$

Initialization

For particles $i = 1, \ldots, N$,

- sample the motion parameters $\boldsymbol{x}_0^i \sim \pi(\boldsymbol{x}_0)$,
- sample the variance vector $\boldsymbol{\phi}_0^i \sim \pi(\boldsymbol{\phi}_0)$.

Iterations

for $t = 1, 2, \ldots$,

- for particles $i = 1, \ldots, N$ and indicator vector $\boldsymbol{\lambda}_t$ values $j = 1, \ldots, n_\Lambda$,
  - * update prior probabilities of the indicator particles, $\mu_t(k)$ and $\gamma_t^i(k)$, for $k = 1, \ldots, n_y$,
  - * sample the motion parameters according to the suboptimal distribution

$$\boldsymbol{x}_{t:t+L}^{i,j} \sim \pi\left(\boldsymbol{x}_{t:t+L} | X_{t-1}^i, \boldsymbol{\lambda}_{t:t+L}^{i,j} = \boldsymbol{\Lambda}_0^j, \boldsymbol{Y}_{t:t+L}\right),$$

  - * sample the variance parameters

$$\boldsymbol{\phi}_t^{i,j} \sim \pi\left(\boldsymbol{\phi}_t | \boldsymbol{x}_{t:t+L}^{i,j}, \boldsymbol{X}_{t-1}^i, \boldsymbol{\lambda}_{t:t+L}^{i,j} = \boldsymbol{\Lambda}_0^j, \boldsymbol{Y}_{t:t+L}\right),$$

  - * extrapolation: for $l = 1, \ldots, L$, $\boldsymbol{\phi}_{t+l}^{i,j} = \boldsymbol{\phi}_t^{i,j}$.
  - * Compute the importance weights $w_{t+l}^{i,j}$ for $l = 0, \ldots, L$.
- Smoothed state estimation

$$\begin{aligned} \boldsymbol{x}_t &= \sum_{i=1}^{N} \sum_{j=1}^{n_\lambda} w_{t+L}^{i,j} \boldsymbol{x}_t^{i,j} \\ \boldsymbol{\phi}_t &= \sum_{i=1}^{N} \sum_{j=1}^{n_\lambda} w_{t+L}^{i,j} \boldsymbol{\phi}_t^{i,j} \end{aligned}$$

- Selection procedure
  - * Perform the hypothesis test

$$\frac{P\left[H_t^1 | \boldsymbol{Y}_{1:t+L}\right]}{P\left[H_t^0 | \boldsymbol{Y}_{1:t+L}\right]} \geq T_h ?$$

  - * Depending on the selected hypothesis, compute the resampling weights $\alpha_t^{i,j}$.
  - * Draw N particles out of $N \times n_\Lambda$ according to the resampling weights. They are denoted $\boldsymbol{S}_{0:t}^i = \left\{\boldsymbol{x}_{0:t}^i, \boldsymbol{\phi}_{0:t}^i, \boldsymbol{\lambda}_{0:t}^i\right\}$ for $i = 1, \ldots, N$.

TABLE I
SUMMARY OF THE PROPOSED FIXED-LAG PARTICLE FILTER.

V. APPLICATION TO A GPS NAVIGATION SCENARIO

A. Simulation settings

Several simulations have been conducted to illustrate the performance of the proposed algorithm. We first consider a trajectory of 200 samples (with a sampling period $T_e = 1$ s) corresponding to a nearly uniform motion with a velocity of 10 m/s. All along this trajectory, the actual distances between the vehicle and the satellites of the GPS constellation have been computed on the basis of GPS almanac files. The latter provide us with the latest upgrades of the satellite orbital parameter values so that we can infer the satellite positions in the ECEF frame of coordinates. Then, we have degraded these ideal pseudoranges by adding both the receiver clock bias, generated according to state model (3), and the measurement noise. The standard deviation of this noise has been adjusted according to RTCA recommendations [1]. Thus it slightly varies over time as a function of the in-view satellite elevation angles. The so-called nominal value of the standard deviation is denoted hereafter $\sigma_t^n(k)$ for the k^{th} satellite at time t. Finally, to simulate the presence of interferences, the pseudoranges associated to the 1^{st} and 2^{nd} in-view satellites (they are referred to as PR 1 and PR 2 in the sequel) have been corrupted by an additive white noise from time instant 67 to time instant 167 for satellite 1 and from time instant 100 to time instant 200 for satellite 2. The standard deviations of these interferences have been chosen so that the overall additive noise does not result in a loss-of-lock of the receiver. Therefore, the following rule-of-thumb has been applied (see [17] for more details): $3\sigma_{\max} = d$, where $\sigma_{\max}$ refers to the maximum tolerable value of the measurement noise standard deviation and d to the correlator spacing. A classical value for the correlator spacing is $\frac{1}{2}$ chip of the PRN code, hence 97 m when considering GPS signals dedicated to civil users. Thus, the maximum value of the standard deviation of the simulated measurement noise is 32.33 m. As a result, the measurement noise standard deviation in the presence of interferences has been set to 25 m for the 1^{st} pseudorange and 30 m for the 2^{nd} pseudorange. Finally, the motion model standard deviation is taken as $\sigma_v = 0.1$ m/s^2 and the clock variance parameters satisfy $S_b = 10^{-19}$ s^2 and $S_d = 3 \times 10^{-19}$ s^2.

B. Simulation results

The performance analysis is conducted in several steps. First, we study the ability of the FLPF to detect variance jumps. For that purpose, we compare the estimated *posterior* probability that a variance jump has occurred with a threshold according to equation (48). Then, we evaluate the accuracy of both the measurement noise variance and the position coordinate estimates in the presence of interferences. Finally, we study the influence of different algorithmic settings such as the parameters of the *prior* distributions and the deterministic exploration strategy. All the results have been obtained by averaging 50 Monte Carlo runs corresponding to different realizations of the measurement noise. For comparison purposes, we have implemented two algorithms in addition to the FLPF

- a fixed-lag smoothing particle filter based on the same Bayesian model and using the test-triggered resampling, but with a random exploration of the discrete-valued states. It should be noted that, for the continuous-valued states, the same proposal distribution as the one presented in section IV is used to propagate the particles.
- a fixed-lag extended Kalman smoother, denoted hereafter FL-EKF, which is coupled with an innovation based hypothesis test to detect the variance jumps. More precisely, among the different algorithms published in the literature, we have implemented the state augmentation smoother which was first proposed by Biswas and Mahalanabis [6] for its numerical stability. The detection of variance jumps is carried out by applying a 2-CUSUM scheme as expressed in [24]. By denoting as $\eta_{i,t}$ the Kalman innovation associated to the i^{th} GPS measurement at time t, the CUSUM statistics are updated as follows

$$C_{i,t}^+ = \max(0, C_{i,t-1}^+) + (\eta_{i,t}^2 - C), \quad (55)$$

$$C_{i,t}^- = \min(0, C_{i,t-1}^-) + (\eta_{i,t}^2 + C), \quad (56)$$

with the initial values $C_{i,0}^+ = C_{i,0}^- = 0$, and C is a threshold which determines the sensitivity of the CUSUM

test to small variance jumps. The absolute values of these statistics are compared to a threshold T_c to detect the variance jumps. Then, a generalized likelihood ratio is used, as presented in [28], to estimate both their times of occurrence and their amplitudes. Finally, the newly estimated values of the GPS measurement noise variance are fed back to the Kalman smoother.

The behavior of the FLPF partly depends on the tuning of different parameters such as the number of particles N and the detection threshold. Their values, as well as the values of the 2-CUSUM scheme, are given in table II for the proposed simulation results. As for the $\mathcal{IG}$ prior distribution parameters, they need to be adjusted on-line since they depend both on the previous value of the measurement noise variance and on the elevation angle of the satellite. For the i^{th} particle and the k^{th} pseudorange at time t, we apply the formula given in section III with the following parameter values

- Case 1 ($\boldsymbol{\lambda}_t^i(k) = 0$): $\sigma_0^{\mathcal{IG}} = 1$ m and $\mu_0^{\mathcal{IG}} = \boldsymbol{\phi}_{t-1}^i(k)$.
- Case 2 ($\boldsymbol{\lambda}_t^i(k) = 1$): the lowest inflexion point is set to $I_{\text{min}} = 12^2$, which is slightly superior to the nominal variance of the GPS measurement noise. The 2^{nd} one is set to $I_{\text{max}} = 32.33^2$ which is the maximum value before loss-of-lock.
- Case 3 ($\boldsymbol{\lambda}_t^i(k) = 2$): $\sigma_2^{\mathcal{IG}} = 1$ m and $\mu_2^{\mathcal{IG}} = \sigma_t^n(k)$, i.e., the nominal value of the measurement noise standard deviation for the k^{th} satellite at time t.

We also study the influence of the lag L by varying its value.

Number of particles	$N = 250$
Penalizing factor	$\beta = 2$
Detection threshold (FLPF)	$T_h = 1$
Detection threshold (CUSUM)	$T_c = 20000$
Sensitivity parameter (CUSUM)	$C = 100$

TABLE II
FLPF AND CUSUM PARAMETERS

1) Variance jump detection: Fig. 2 shows the number of detections at each time step over the 50 Monte Carlo runs. For that purpose, we apply the Bayesian hypothesis test (48) with a threshold $T_h = 1$ (maximum *a posteriori* rule) and we set $L = 8$. We can observe that almost all the detections are located at the vicinity of the actual variance changepoints, which are indicated by vertical dashed lines. However, due to the fixed-lag smoothing, the variance jumps may be detected a few time steps before they actually occur. To study the influence of the lag, we have computed the statistics of the detection delay for different values of L indicated in table III. The results obtained with $L = 2$ have not been reported because the missed and false detections were too numerous to compute significant statistics. Broadly speaking, the higher the lag, the higher the bias in the estimated changepoint because the detection occurs systematically before the actual changepoint. Conversely, the standard deviation of the detection delay decreases with L because the detection becomes less sensitive to the measurement noise. It should be noted that a lag $L = 5$ seems to offer a good compromise between

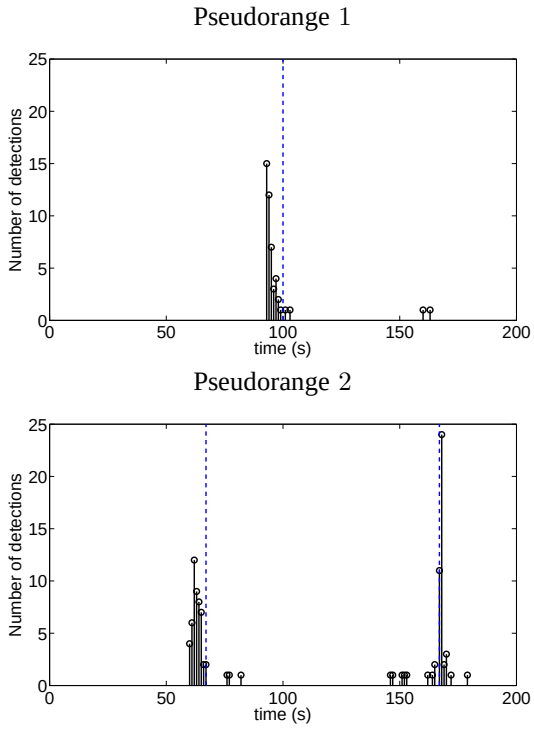

Fig. 2. *Posterior* number of detections over the 50 Monte Carlo runs for pseudorange 1 (top) and pseudorange 2 (bottom).

	Changepoints	$t = 67$ s (PR 1)	$t = 100$ s (PR 2)	$t = 167$ s (PR 1)
Lag = 8	Detection delay (s)	-3.5	-5	1.4
	Standard deviation (s)	2.3	1.9	3.4
Lag = 5	Detection delay (s)	-1	-1.9	2.1
	Standard deviation (s)	2.7	2.1	3.8

TABLE III
MEAN DETECTION DELAY AND STANDARD DEVIATION OF THE DETECTION DELAY IN S FOR DIFFERENT CHANGEPOINTS AND DIFFERENT VALUES OF THE LAG L.

bias and variance when considering changepoint estimation. However, better results are obtained with a lag $L = 8$ for estimating the variance jump amplitudes as shown in the next section.

2) Variance estimation: Fig. 3 shows the average of the FLPF measurement noise standard deviation estimates obtained from 50 Monte Carlo runs. Different values of the lag L have been considered to emphasize the benefits of smoothing. It can be noted that the estimated curve that best fits the actual value of the standard deviation is obtained for $L = 8$. However, due to smoothing, the value of the estimated standard deviation starts increasing a few time steps before the actual changepoint. With a lag $L = 5$, the FLPF tends to slightly overestimate the value of the standard deviation after the jump but still achieves a good trade-off between accuracy and computational complexity. On the contrary, with a too small value of the lag ($L = 2$), the proposed algorithm does have enough information from the measurements to

counterbalance the vague *prior* distribution assigned to the variance value in the presence of a jump. In this case, the FLPF yields too high values of the standard deviation. Therefore, due to the uncertainty on the variance jump amplitude, smoothing turns out to be necessary to properly track the variance value.

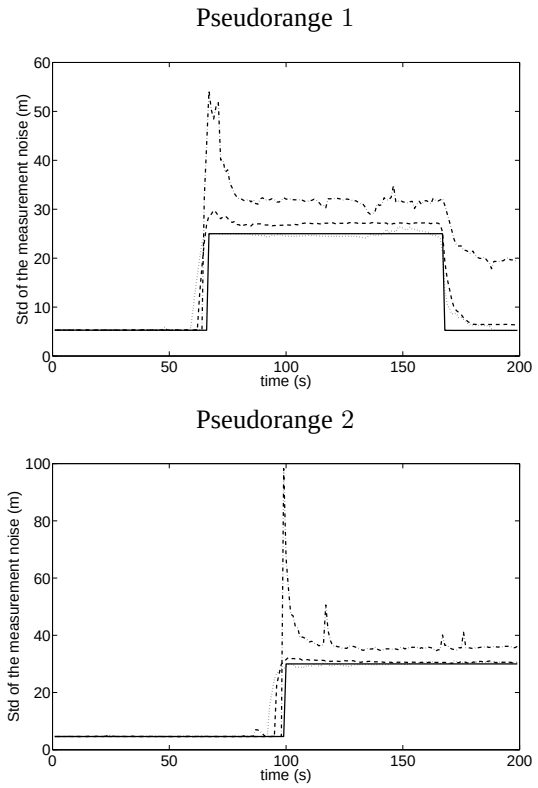

Fig. 3. Average of the FLPF measurement noise standard deviation (std) estimates, computed from 50 MC runs. Plain line: actual values, dotted line: $L = 8$, dashed line: $L = 5$, dashdot line: $L = 2$.

3) Positioning error: In order to appreciate the interest of the proposed algorithm in term of positioning error, Fig. 4 shows the root mean square error (RMSE) between the true position of the mobile and the estimates obtained with the FLPF and the FL-EKF using the same lag $L = 8$. Before the appearance of the interferences, the FL-EKF RMSEs are slightly inferior to that of the FLPF, most presumably due to the limited number of particles used in the FLPF implementation. On the contrary, after the appearance of the interferences, the FLPF yields the lowest RMSEs. When comparing both algorithms, it appears that the FPLF positioning error can be locally decreased up to 5 meters with respect to the FL-EKF. A closer analysis shows that the 2-CUSUM test timely detects the jumps. However, their amplitudes may be poorly estimated, which in return degrades the navigation state estimates. Furthermore, the gain in accuracy achieved with the FLPF is expected to be more significant for longer interference periods.

Another way of comparing the different navigation algorithms consists of computing Bayesian confidence intervals, or so-called credible intervals [25], for the different estimates. Fig. 5 shows the x-coordinate estimation error versus time and the approximate credible intervals, defined by twice the estimated standard deviation of the estimation error, for the FL-EKF and the FLPF. The FLPF credible intervals are more in agreement than the FL-EKF ones with the corresponding positioning errors. Thus, an additional advantage of the proposed approach is to provide interesting uncertainty measures for the positioning errors along the trajectory. Furthermore, we

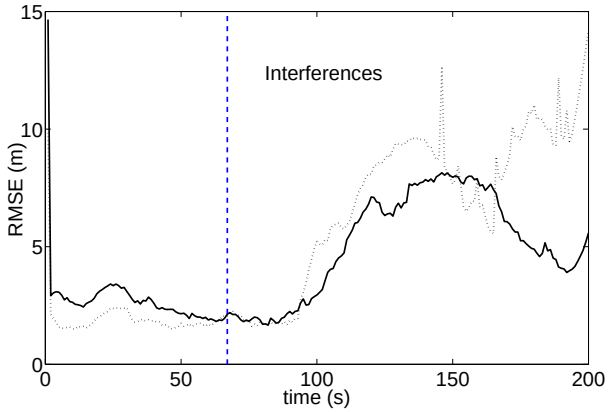

Fig. 4. RMSEs for the position estimation. Plain line : FLPF, dotted line : FL-EKF. Vertical dashed lines: variance changepoints.

TABLE IV
RMSEs (M) FOR THE X,Y AND Z COORDINATES WITH DIFFERENT LAGS. $^{(1)}$: WITHOUT THE HYPOTHESIS TEST, $^{(2)}$: WITH THE HYPOTHESIS TEST.

(a) Positioning errors with respect to the true mobile trajectory.

	$L = 8^{(1)}$	$L = 8^{(2)}$	$L = 5^{(2)}$	$L = 2^{(2)}$
x axis	5.04	4.40	5.24	10.43
y axis	5.26	4.68	5.53	10.52
z axis	7.65	6.93	7.81	14.9

(b) Positioning errors with respect to the mean of the fixed lag distribution.

	$L = 8^{(1)}$	$L = 8^{(2)}$	$L = 5^{(2)}$	$L = 2^{(2)}$
x axis	4.46	4.32	5.24	8.96
y axis	4.82	4.85	5.43	9.20
z axis	7.40	7.31	8.17	13.19

have studied the influence of both the lag and the hypothesis test on the positioning error. Table IV(a) reports the RMSEs for the x, y and z coordinates for different values of the lag L. The lowest RMSEs are obtained with the lag $L = 8$. For this value, using the hypothesis test clearly allows one to reduce the estimation error. The same remark holds for $L = 5$ and $L = 2$ but the RMSE in the absence of hypothesis test have not been reported in the table for the sake of brevity. By speeding up the removal of non relevant particles after a variance jump, the hypothesis test improves the variance estimation during the time intervals associated to interferences.

Finally, to take into account that we compute an approximation of the means of the smoothing distribution and not the exact values of the hidden Markov chain $\{\boldsymbol{X}_t\}_{t\geq 0}$, we have also evaluated the RMSEs between the algorithm estimates and the estimates obtained by running a reference particle filter using $100,000$ particles. These errors are provided in table IV(a). They are very close to the RMSEs reported in table IV(b), which ensures that the exact position coordinates of

the mobile coincide with the means of the smoothing *posterior* distribution.

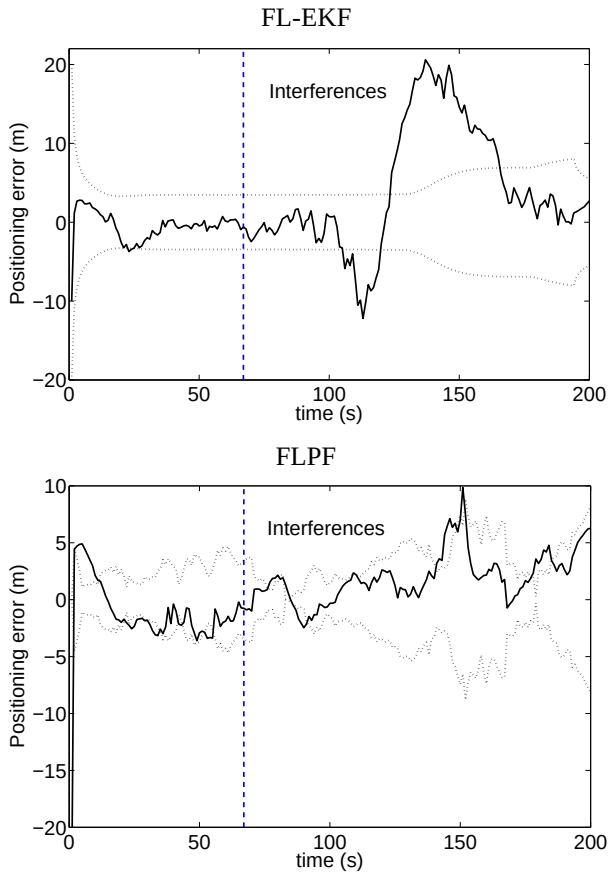

Fig. 5. Positioning error (plain line) and 95% confidence bounds for the FL-EKF and the FLPF. The variance changepoints are indicated by vertical dashed lines.

4) Deterministic versus random exploration: Following results previously published in the litterature [22] [27] [13], we have favored a deterministic scheme for the exploration of the discrete-valued states. In order to study the relevance of this approach, we have also implemented the proposed algorithm with a random evolution of all the unknown parameters. Since n_λ offsprings are considered per particle for the deterministic technique, the fully random scheme is implemented with $N \times n_\lambda$ particles so that the overall number of particles used for the estimation is the same.

Table V presents the number of good detections over 50 Monte Carlo runs for the different variance jumps. As expected, the exhaustive exploration technique outperforms a fully random approach when dealing with the estimation of the discrete-valued indicator vector $\boldsymbol{\lambda}_t$. However, this result is somewhat counterbalanced by the positioning RMSEs which are plotted in Fig. 6. It appears that the RMSEs of the fully random PF are slightly inferior to that of the combined random/deterministic PF. This last result can be explained as follows. The combined random/deterministic PF allocates a fixed number of particles N to each scenario: slow evolution of the noise variance or abrupt jump. Since the variance shifts are rare events which have a small *prior* probability, most of the standard PF particles correspond to the 1^{st} scenario.

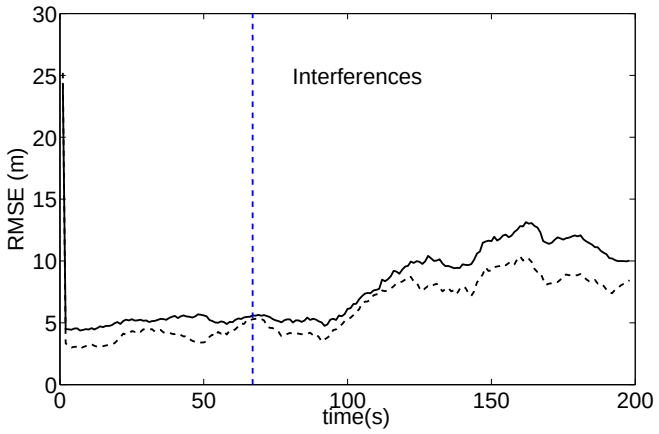

Fig. 6. Positioning RMSEs for the combined deterministic/random exploration scheme (plain line) and the fully random scheme (dashed line).

Thus, most of the time (99% of the time in the simulation), only N particles of the combined deterministic/random PF are actually useful for the estimation, which should be compared to nearly $N \times n_\lambda$ for the standard PF. Conversely, at each changepoint, the number of particles indicating the variance shift is far more important when considering in a systematic manner all the indicator vector possible values.

Finally, to make the analysis complete, it should be noted that the computational complexity between the compared algorithms is not strictly equivalent. The resampling step, which is quite demanding, involves only N particles for the combined deterministic/random PF against $N \times n_\lambda$ for the fully random algorithm. To conclude, the combined deterministic/random strategy is more efficient for detecting the presence of interferences. However, a fully random strategy might be considered if we are only interested in positioning errors.

Changepoints	$t = 67$ s (PR 1)	$t = 100$ s (PR 2)	$t = 167$ s (PR 1)
Combined deterministic/random exploration	50	48	40
Random exploration	42	39	42

TABLE V
NUMBER OF GOOD DETECTIONS OVER 50 MONTE CARLO RUNS FOR THE DIFFERENT CHANGEPOINTS .

C. Sensitivity to parameter tuning

Fig. 7 investigates the robustness of the FLPF with respect to some user-chosen parameters. First of all, the frequency of the variance jumps is determined by the parameter γ. In the considered simulation setting, the actual value of γ is 0.01. Fig. 7a) depicts the positioning RMSEs obtained by considering different values of γ in the FLPF implementation. These RMSEs are computed by averaging the positioning error over 50 Monte Carlo runs and over the 200 points of the mobile trajectory. Unsurprisingly, the minimum error is obtained when using the true value of γ. However, varying γ

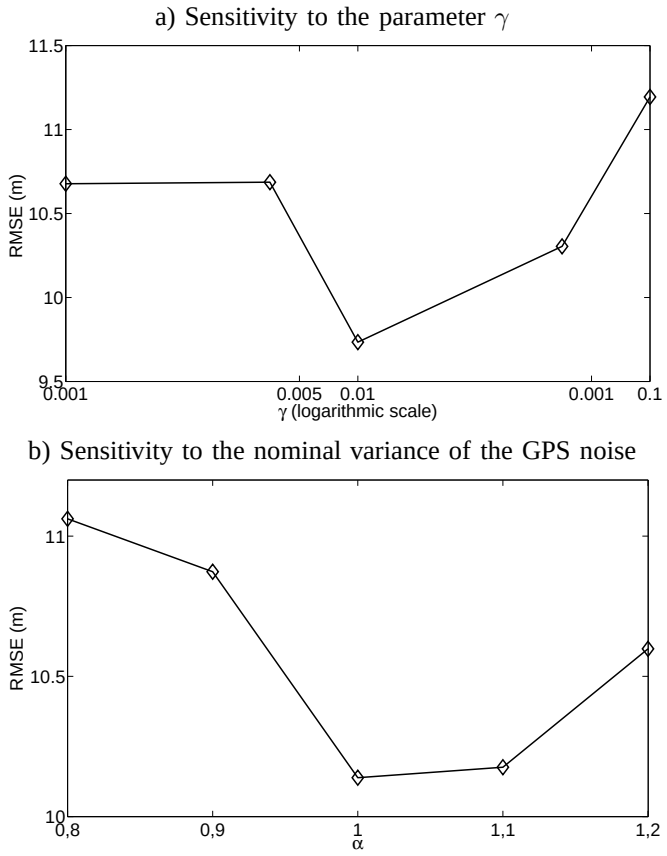

Fig. 7. Positioning RMSEs for different tuning of the FLPF parameters.

does not impact significantly the FLPF performance, probably due to the deterministic exploration strategy.

Then, it is worth studying the sensitivity of the algorithm to the parameters of the $\mathcal{IG}$ distributions assigned to the variance states. When considering the 3 cases presented in section III.C, it appears that the *prior* distribution is relatively non informative in case 2. On the contrary, in cases 1 and 3, the shape of the variance *prior* distributions is directly impacted by the nominal GPS noise standard deviation, denoted $\sigma_t^n(k)$ for the k^{th} pseudorange at time t. Fig 7b) illustrates the robustness of the FLPF with regards to an imperfect knowledge of $\sigma_t^n(k)$. This figure shows the RMSEs obtained with different values of α, which is the ratio between the true value of the observation noise standard deviation and the value considered in the FLPF implementation. Again, the best positioning accuracy is achieved by using the true value of the $\sigma_t^n(k)$ (corresponding to $\alpha = 1$). Although this parameter appears to impact more significantly the FLPF than γ, the proposed algorithm seems quite robust to uncertainties. In addition, it should be noted that a too erroneous value of $\sigma_t^n(k)$ would be detected as a variance jump. Thus, its influence on the RMSE would be attenuated.

VI. Conclusion

This paper addressed the problem of mitigating RF interferences in GPS navigation. Contrary to existing approaches, the proposed algorithm directly compensated for the interferences effects at the level of the navigation algorithm. For that purpose, interferences were modeled as variance jumps affecting the GPS measurements. A particle filtering algorithm was then proposed to estimate these variance jumps jointly with the vehicle motion. In order to improve the variance jump detection, several alternatives to the classical particle filter were introduced. First, the sparsity of interferences was taken into account to perform smoothing while preserving a reasonable computational complexity. Second, an efficient proposal distribution was introduced to capture the information brought by the current measurements when simulating the particles. Finally, an hypothesis test was introduced at the level of the resampling step to accelerate the removal of irrelevant particles. The performance of the so-called FLPF was validated on simulated data.

We are currently investigating the following extensions. First, this study assumed that interferences corrupting the different pseudoranges were not correlated. This hypothesis makes easier the definition of indicator *priors* but may be restrictive in some practical applications. An alternative would be to consider that measurements resulting from a set of satellites located in the same direction are likely to experience interferences at the same time. For that purpose, correlations between the components of $\boldsymbol{\lambda}_t$ should be introduced, e.g. by defining appropriate *prior* distributions for this vector. Improving detection by exploiting the correlation between multiple measurements has already shown interesting results in other contexts such as the joint segmentation of multiple time series [12] [11]. We think this strategy can also be useful for navigation applications.

Appendix A
Proposal distribution

This appendix derives the proposal distribution of the mobile motion parameters used in the proposed particle filtering algorithm. As mentioned in section IV, the optimal proposal distribution (in the sense that it minimizes the variance of the PF importance weights) is

$$p\left(\boldsymbol{x}_{t:t+L}|\boldsymbol{X}_{t-1}^i, \boldsymbol{\lambda}_{t:t+L}^{i,j} = \boldsymbol{\Lambda}_0^j, \boldsymbol{Y}_{t:t+L}\right). \tag{57}$$

This distribution can be obtained by marginalization as follows

$$\begin{aligned} &p\left(\boldsymbol{x}_{t:t+L}|\boldsymbol{X}_{t-1}^i, \boldsymbol{\lambda}_{t:t+L}^{i,j} = \boldsymbol{\Lambda}_0^j, \boldsymbol{Y}_{t:t+L}\right) \\ &= \int p\left(\boldsymbol{x}_{t:t+L}, \boldsymbol{\phi}_t|\boldsymbol{X}_{t-1}^i, \boldsymbol{\lambda}_{t:t+L}^{i,j} = \boldsymbol{\Lambda}_0^j, \boldsymbol{Y}_{t:t+L}\right) d\boldsymbol{\phi}_t. \end{aligned} \tag{58}$$

Then, by applying several times Bayes' rule, the joint distribution of the continuous states can be decomposed in the following manner

$$\begin{aligned} &p\left(\boldsymbol{x}_{t:t+L}, \boldsymbol{\phi}_t|\boldsymbol{X}_{t-1}^i, \boldsymbol{\lambda}_{t:t+L}^{i,j} = \boldsymbol{\Lambda}_0^j, \boldsymbol{Y}_{t:t+L}\right) \\ &\propto p\left(\boldsymbol{Y}_{t:t+L}|\boldsymbol{x}_{t:t+L}, \boldsymbol{\phi}_t\right) p\left(\boldsymbol{x}_{t:t+L}|\boldsymbol{x}_{t-1}^i\right) p\left(\boldsymbol{\phi}_t|\boldsymbol{\phi}_{t-1}^i, \boldsymbol{\lambda}_t^{i,j}\right) \\ &\propto p\left(\boldsymbol{x}_{t:t+L}|\boldsymbol{x}_{t-1}^i\right) \prod_{k=1}^{n_y} \frac{\mathcal{IG}\left(\boldsymbol{\phi}_t(k); \tilde{\alpha}_t^{i,j}(k), \tilde{\beta}_t^{i,j}(k)\right)}{\left(\tilde{\beta}_t^{i,j}(k)\right)^{\tilde{\alpha}_t^{i,j}(k)}} \end{aligned} \tag{59}$$

where the expressions of $\tilde{\alpha}_t^{i,j}(k)$ and $\tilde{\beta}_t^{i,j}(k)$ are given by (40) and (41). It should be noted that, in the above decomposition,

we have considered that the variance remains constant for $l = 0, \ldots, L$.

By integrating out the variance states, we can obtain an analytical expression of the optimal proposal distribution

$$\begin{aligned} & p\left(\boldsymbol{x}_{t:t+L}|\boldsymbol{X}_{t-1}^{i}, \boldsymbol{\lambda}_{t:t+L}^{i,j} = \boldsymbol{\Lambda}_{0}^{j}, \boldsymbol{Y}_{t:t+L}\right) \\ & \propto p\left(\boldsymbol{x}_{t:t+L}|\boldsymbol{x}_{t-1}^{i}\right) \prod_{k=1}^{n_y} \left(\tilde{\beta}_{t}^{i,j}(k)\right)^{-\tilde{\alpha}_{t}^{i,j}(k)} \\ & \propto p\left(\boldsymbol{x}_{t:t+L}|\boldsymbol{x}_{t-1}^{i}\right) \prod_{k=1}^{n_y} T_{t}^{i,j}(k) \end{aligned} \tag{60}$$

where

$$\begin{aligned} T_{t}^{i,j}(k) &= \left(1 + \frac{u_{t}^{i,j}(k)}{2\alpha\left(\boldsymbol{\Lambda}^{\boldsymbol{j}}(\boldsymbol{k})\right) + L}\right)^{-\frac{2\alpha\left(\boldsymbol{\Lambda}^{\boldsymbol{j}}(\boldsymbol{k})\right)+L+1}{2}} \\ u_{t}^{i,j}(k) &= \sqrt{\frac{\sum_{l=0}^{L}\left(\boldsymbol{Y}_{t+l}(k) - \boldsymbol{h}_{t+l}^{k}\left(\boldsymbol{x}_{t+l}\right)\right)^{2}}{\frac{2\beta\left(\boldsymbol{\Lambda}^{\boldsymbol{j}}(\boldsymbol{k})\right)}{2\alpha\left(\boldsymbol{\Lambda}^{\boldsymbol{j}}(\boldsymbol{k})\right)+L}}}. \end{aligned} \tag{61}$$

$T_{t}^{i,j}(k)$, as defined in (61), takes the form of a Student distribution with $2\alpha\left(\boldsymbol{\Lambda}^{\boldsymbol{j}}(\boldsymbol{k})\right) + L$ degrees of freedom, which is evaluated in $u_{t}^{i,j}(k)$. Student distributions are centered, symmetric and bell-shaped distributions similar to Gaussian distributions. However, their tails are heavier. The higher the degree of freedom, the closer the Student distribution to a Gaussian distribution. To derive a Gaussian proposal distribution for the mobile motion vector, we propose here to approximate $T_{t}^{i,j}(k)$ as follows

$$\begin{aligned} T_{t}^{i,j}(k) &\simeq \frac{1}{\sqrt{2\pi}} \exp\left(-\frac{u_{t}^{i,j}(k)^{2}}{2}\right) \\ &\propto \exp\left(-\frac{\sum_{l=0}^{L}\left(\boldsymbol{Y}_{t+l}(k) - \boldsymbol{h}_{t+l}^{k}\left(\boldsymbol{x}_{t+l}\right)\right)^{2}}{2\boldsymbol{V}_{t}^{i,j}(k)}\right) \end{aligned} \tag{62}$$

where the parameter $\boldsymbol{V}_{t}^{i,j}(k)$ is defined as

$$\boldsymbol{V}_{t}^{i,j}(k) = \frac{\alpha\left(\boldsymbol{\Lambda}^{\boldsymbol{j}}(\boldsymbol{k})\right) + L/2}{\beta\left(\boldsymbol{\Lambda}^{\boldsymbol{j}}(\boldsymbol{k})\right)}. \tag{63}$$

By substituting (62) in (61), we obtain the following approximation of the proposal distribution

$$\begin{aligned} & p\left(\boldsymbol{x}_{t:t+L}|\boldsymbol{X}_{t-1}^{i}, \boldsymbol{\lambda}_{t:t+L}^{i,j} = \boldsymbol{\Lambda}_{0}^{j}, \boldsymbol{Y}_{t:t+L}\right) \\ & \propto p\left(\boldsymbol{x}_{t:t+L}|\boldsymbol{x}_{t-1}^{i}\right) \prod_{k=1}^{n_y} \prod_{l=0}^{L} f_{t}^{k}(\boldsymbol{x}_{t+l}) \end{aligned} \tag{64}$$

with

$$f_{t}^{k}(\boldsymbol{x}_{t+l}) = \exp\left(-\frac{\left(\boldsymbol{Y}_{t+l}(k) - \boldsymbol{h}_{t+l}^{k}\left(\boldsymbol{x}_{t+l}\right)\right)^{2}}{2\boldsymbol{V}_{t}^{i,j}(k)}\right). \tag{65}$$

The distribution (64) is still not easy to simulate. Thus, we propose to generate one after the other the motion vectors $\boldsymbol{x}_{t+l}^{i,j}$, for $l = 0, \ldots, L$, by using a Gaussian approximation of (64). For that purpose, we perform a local linearization of the GPS observation equation so as to express, up to a proportionality constant, the function $f_{t}(\boldsymbol{x}_{t+l})$ as a Gaussian distribution with regards to $\boldsymbol{x}_{t+l}$. This linearization leads to

$$\boldsymbol{h}_{t+l}\left(\boldsymbol{x}_{t+l}\right) \simeq \boldsymbol{h}_{t+l}\left(F\boldsymbol{x}_{t+l-1}^{i,j}\right) + H_{t+l}^{i,j}\left(\boldsymbol{x}_{t+l} - F\boldsymbol{x}_{t+l-1}^{i,j}\right)$$

for $l = 0, \ldots, L$, where $\boldsymbol{x}_{t+l}$ is the actual motion vector and $H_{t+l}^{i,j}$ refers to the matrix of the partial derivatives of the function $\boldsymbol{h}_{t+l}$ with respect to the components of $\boldsymbol{x}_{t+l}$, evaluated in $F\boldsymbol{x}_{t+l-1}^{i,j}$.

We can take advantage of this linearization to rewrite $f_{t}(\boldsymbol{x}_{t+l})$ as follows

$$f_{t}^{k}(\boldsymbol{x}_{t+l}) \simeq \exp\left(-\frac{\left(\Delta\boldsymbol{Y}_{t+l}^{i,j}(k) - H_{t+l}^{i,j}(k,:)\boldsymbol{x}_{t+l}\right)^{2}}{\boldsymbol{V}_{t+l}^{i,j}(k)}\right)$$

where $H_{t+l}^{i,j}(k,:)$ stands for the k^{th} row of matrix $H_{t+l}^{i,j}$. Thus, it becomes possible to simulate the motion vector $\boldsymbol{x}_{t+l}^{i,j}$ according to the Gaussian distribution

$$\begin{aligned} & \pi\left(\boldsymbol{x}_{t+l} \;|\boldsymbol{S}_{t-1}^{i}, \boldsymbol{\lambda}_{t:t+l}^{i,j}, \boldsymbol{x}_{t+l-1}^{i,j}, \boldsymbol{Y}_{1:t+l}\right) \\ & \qquad = \mathcal{N}\left(\boldsymbol{x}_{t+l}; \boldsymbol{m}_{t+l}^{i,j}, \Sigma_{t+l}^{i,j}\right) \end{aligned} \tag{66}$$

with mean and covariance matrix defined as

$$\begin{aligned} \Sigma_{t+l}^{i,j} &= \left(\left(H_{t+l}^{i,j}\right)^{T}\left(D_{t}^{i,j}\right)^{-1} H_{t+l}^{i,j} + Q\right)^{-1} \\ \boldsymbol{m}_{t+l}^{i,j} &= \Sigma_{t+l}^{i,j}\left(Q^{-1}F\boldsymbol{x}_{t+l-1}^{i,j} + \left(D_{t}^{i,j}\right)^{-1}\left(H_{t+l}^{i,j}\right)^{T}\Delta\boldsymbol{Y}_{t+l}^{i,j}\right) \end{aligned}$$

where $D_{t}^{i,j} = \text{diag}\left(\boldsymbol{V}_{t}^{i,j}\right)$ and

$$\Delta\boldsymbol{Y}_{t+l}^{i,j} = \boldsymbol{Y}_{t+l} - \boldsymbol{h}_{t+l}\left(F\boldsymbol{x}_{t+l-1}^{i,j}\right) - H_{t+l}^{i,j}F\boldsymbol{x}_{t+l-1}^{i,j}.$$

ACKNOWLEDGMENT

The authors would like to thank Vincent Calmettes, Anne-Christine Escher and André Monin for fruitful discussions about this work.

REFERENCES

[1] RTCA document no. RTCA/DO-229b. *Minimum Operational performance standards for Global Positioning System/Wide-Area Augmentation Systems Airborne equipment*.

[2] S. Alban, D. M. Akos, S. M. Rock, and D. Gebre-Egziabher. Performance analysis and architectures for INS-aided GPS tracking loops. In *Proc. ION NTM*, Anaheim, CA, Jan. 22–24, 2003.

[3] C. Andrieu and A. Doucet. Joint Bayesian model selection and estimation of noisy sinusoids via reversible jump MCMC. *IEEE Trans. on Signal Process.*, 47(10):2667–2676, 1999.

[4] S. Arulampalam, S. Maskell, and N. Gordon. A tutorial on particle filters for online nonlinear/non-Gaussian Bayesian tracking. *IEEE Trans. on Signal Process.*, 50(2):174–188, February 2002.

[5] J. W. Betz and K. R. Kolodziejski. Extended theory of early-late code-tracking for a band-limited GPS receiver. *NAVIGATION, Journal of the Institute of Navigation*, 47(3):211–226, Fall 2000.

[6] K. K. Biswas and A. K. Mahalanabis. Optimal fixed-lag smoothing for time-delayed systems with colored noise. *IEEE Trans. on Autom. Cont.*, 17:387–388, 1972.

[7] R. G. Brown and P. Hwang. GPS failure detection by autonomous means within the cockpit. In *Proc. ION NTM*, Seattle, WA, June 24–26, 1986.

[8] R. G. Brown and P. Y. C. Hwang. *Introduction to Kalman signals and applied Kalman filtering*. Wiley, 3^{rd} edition, 1994.

[9] O. De Cambry. Segmentation de signaux sous contrainte de longueur minimale. In *Proc. of Gretsi*, Toulouse, 10–13 Sept, 2001.

[10] R. Van der Merwe, N. de Freitas A. Doucet, and E. Wan. *The unscented particle filter*. MIT Press, Eds: T.K. Leen, T.G. Dietterich, and V. Tresp, Dec 2000.

[11] N. Dobigeon, J. Y. Tourneret, and M. Davy. Joint segmentation of piecewise constant autoregressive processes by using a hierarchical model and a Bayesian sampling approach. *IEEE Trans. on Signal Process.*, 55(4):1251–1263, April 2007.

[12] N. Dobigeon, J. Y. Tourneret, and J. D. Scargle. Joint segmentation of multivariate astronomical time series: Bayesian sampling with a hierarchical model. *IEEE Trans. on Signal Process.*, 55(2):414–423, February 2007.

[13] B. Dong, X. Wang, and A. Doucet. A new class of soft MIMO demodulation algorithms. *IEEE Trans. on Signal Process*, 51(11):2752–2763, 2003.

[14] A. Doucet, N. de Freitas, and N. Gordon. *Sequential Monte Carlo methods in practice*. Springer-Verlag, New York, WA, 2001.

[15] A. Giremus, J. Y. Tourneret, and V. Calmettes. A particle filter approach for joint detection/estimation of multipath effects on GPS measurements. *IEEE Trans. on Signal Process.*, 54(12):1275–1285, April 2006.

[16] N. J. Gordon, D. J. Salmond, and A. F. M. Smith. Novel approach to nonlinear/non-Gaussian bayesian state estimation. *IEE Proceedings on Radar and Signal Process.*, 140(2):107–113, April 1993.

[17] E. D. Kaplan. *Understanding GPS, principles and applications*. Artech House, Boston, MA, 1996.

[18] Y. C. Lee. Analysis of the range and position comparison methods as a means to provide GPS integrity in the user receiver. In *Proc. ION NTM*, Seattle, WA, June 24–26, 1986.

[19] X. Rong Li and V. P. Jilkov. Survey of maneuvring target tracking, part i: dynamic models. *IEEE Trans. Aerosp. Electron. Syst.*, 39(4):1333–1364, October 2003.

[20] J. S. Liu and R. Chen. Blind deconvolution via sequential imputation. *J. Amer. Statist. Assoc.*, 90(430):567–576, 1995.

[21] M. Nicoli, C. Morelli, and V. Rampa. A jump Markov particle filter for localization of moving terminals in dense multipath indoor scenarios. *IEEE Trans. on Signal Process*, 56(8):3801–3809, 2008.

[22] E. Punskaya. *Sequential Monte Carlo methods for digital communications*. PhD thesis, Cambridge University Engineering Department, 2003.

[23] E. Punskaya, C. Andrieu, A. Doucet, and W. J. Fitzgerald. Bayesian curve fitting using MCMC with applications to signal segmentation. *IEEE Trans. on Signal Process*, 50(3):747–758, 2002.

[24] M. R. A. Reynolds and Z. G. Stoumbos. Should observations be grouped for effective process monitoring. *Journal of Quality Technology*, 36(343–366), 2004.

[25] C.P. Robert. *The Bayesian choice: from decision-theoretic foundations to computational implementation*. Springer-Verlag, New York, WA, 2001.

[26] M. Sahmoudi and M. G. Amin. Optimal robust beamforming for interference and multipath mitigation in GNSS arrays. In *Proc. IEEE ICASSP-07*, Honolulu, Hawaii, Apr. 15–20, 2007.

[27] G. Salut and F. Ben Salem. Deterministic particle receiver for multipath fading channels in wireless communications, Part I:FDMA. *Traitement du Signal*, 21(4):347–358, 2004.

[28] M. Spangenberg, J.Y. Tourneret, V. Calmettes, and G. Duchâteau. Detection of variance changes and mean value jumps in measurement noise for multipath mitigation in urban navigation. In *Proc. of 42nd Asilomar conference on Signals, Systems and Computers*, pages 1193–1197, 2008.

[29] K. Vanderwerf. FDE using multiple integrated GPS/inertial Kalman filters in the presence of temporally and spatially correlated ionospheric errors. Salt Lake City, UT, Sept 11–14, 2001.

[30] X. Wang, R. Chen, and D. Guo. Delayed-pilot sampling for mixture Kalman Filter with application in fading channels. *IEEE Trans. on Signal Process.*, 50(2):241–254, February 2002.

[31] P. W. Ward. Advanced GPS receiver systems. *Navtech Seminars*, 1, February 1994.

[32] P. W. Ward. GPS Receiver RF interference monitoring, mitigation and analysis techniques. *NAVIGATION, Journal of the Institute of Navigation*, 41(4):367–391, Winter 1994.

[33] V. S. Zaritskii, V. B. Svetnik, and L. I. Shimelevich. Monte Carlo technique in problems of optimal data processing. *Auto. Remot. Cont.*, 12:95–103, 1975.